Computation of Phase Transformation Paths in Steels by a Combination of the Partial- and Para-equilibrium Thermodynamic Approximations

Takao Koshikawa, Charles-André Gandin, Michel Bellet, Hideaki Yamamura, Manuel Bobadilla

Computation of Phase Transformation Paths in Steels by a Combination of the Partial- and Para-equilibrium Thermodynamic Approximations

Takao KOSHIKAWA,[1,2]* Charles-André GANDIN,[1] Michel BELLET,[1] Hideaki YAMAMURA[3] and Manuel BOBADILLA[4]

1) MINES ParisTech & CNRS, CEMEF UMR 7635, 06904 Sophia Antipolis, France.
2) Nippon Steel & Sumitomo Metal Corporation, Oita Works Equipment Division, 1 Oaza-Nishinosu, Oita City, Oita Prefecture, 870-0992 Japan.   3) Nippon Steel & Sumitomo Metal Corporation, Steelmaking R&D Division, 20-1 Shintomi, Futtsu City, Chiba Prefecture, 293-8511 Japan.
4) ArcelorMittal Maizières, Research and Development, BP 30320, 57283 Maizières-lès-Metz Cedex, France.

A model combining the partial-equilibrium and para-equilibrium thermodynamic approximations is presented. It accounts for fast diffusion of interstitial elements, such as carbon, and low diffusion of substitutional elements in the solid phases, while complete mixing is assumed for all elements in the liquid phase. These considerations are turned into classical mathematical expressions for the chemical potentials and the u-fractions, to which mass conservation equations are added. The combination of the two models permits application to steels, dealing with partial-equilibrium for solidification and para-equilibrium for both the δ-BCC to γ-FCC peritectic transformation and the γ-FCC to α-BCC solid state transformation. The numerical scheme makes use of calls to Thermo-Calc and the TQ-interface for calculating thermodynamic equilibrium and accessing data from the TCFE6 database. Applications are given for a commercial steel. The results are discussed based on comparison with classical microsegregation models and experimental data.

KEY WORDS: solidification; microsegregation; partial-equilibrium; para-equilibrium; peritectic transformation.

1. Introduction

Average alloy properties in multiphase temperature intervals are important for thermomechanical process simulations. Numerical tools have been developed to follow the transformation paths based on thermodynamic considerations. Two classical limits are routinely computed: the lever rule (LR) approximation and the Gulliver-Scheil (GS) approximation.[1,2] For LR, full equilibrium is assumed, meaning that all chemical elements can diffuse rapidly. In contrast, the GS approximation neglects diffusion in solid phases where elements are completely frozen. In practice, most industrial steels include interstitial and substitutional elements. Interstitial elements, such as carbon, have high diffusivity in the solid phase while substitutional elements have low diffusivity. Thus, the above LR and GS approximations do not fully apply. To overcome this problem, the partial-equilibrium (PE) approximation[3,4] has been developed. PE is intended to take into account perfect diffusion of interstitial elements but no diffusion of substitutional elements. However, the peritectic transformation often encountered in commercial alloys cannot take place if only PE is

considered. This limitation could be circumvented by a LR treatment of the δ-BCC (or δ-ferrite)/γ-FCC (or γ-austenite) mixture during the peritectic transformation,[5] thus permitting the activation of the δ-BCC to γ-FCC phase transformation. This will be later refereed as PE + LR solidification path. It is to be mentioned that, while in agreement with observations, no experimental quantitative data is yet available that could be directly compared with predicted kinetics of the peritectic phase transformation. The LR treatment of the peritectic transformation is also a very crude approximation that does not fix the problem in coherent manner with respect to the PE approximation.

In the present study, a new numerical scheme is presented for the computation of phase transformations in steels. It is coupled with thermodynamic equilibrium calculations based on call to the software Thermo-Calc[6] through the TQ-interface using the TCFE6 database.[7] The so-called para-equilibrium (PA) approximation presented by Hillert[8] has been introduced to deal with the peritectic reaction during a PE solidification path, later refereed as PE + PA approximation. This is implemented in previous developments presented by Zhang et al.[4] for the computation of LR, GS and PE + LR solidification paths. Because PA was initially developed for solid state transformations, it is also used to simulate phase transformations during cooling expe-

* Corresponding author: E-mail: takao.koshikawa@mines-paristech.fr

rienced during steel processing after solidification. The numerical scheme is applied to steel alloys experiments also presented in this contribution.

2. Experiments

2.1. Unidirectional Solidification Experiment

To investigate solidification path in Fe–C–Mn–S–Si–P–Al steels, Bridgman solidification experiments have been carried out. The principle of this classical method is explained elsewhere.[9,10] The sample is prepared with a 1 kg furnace. The nominal composition of the investigated alloy S-1 is shown in **Table 1**. The specimen was shaped to 5 mm diameter rod. After setting the sample to the apparatus, it was heated over the liquidus temperature in the hot zone of the Bridgman apparatus and then withdrawn at a constant velocity toward the cold zone, thus achieving solidification. The velocity was set to $8 \cdot 10^{-5}$ m s^{-1}. The measured temperature gradient along the main longitudinal axis of the sample reached 30°C cm^{-1} during the experiment. The sample was finally quenched while still mushy in order to abruptly solidify the remaining liquid. One could thus distinguish the remaining liquid quenched into a fine microstructure from the solid phase formed before quenching. The sample was cut along transverse sections at various heights along the rod axis. The fraction of the solid phase formed before quenching was then estimated by means of image analysis at each transverse section. The evolution of the solid fraction versus position along the length of the rod could be deduced. Using the temperature gradient, the length was converted into a temperature. A profile of solid fraction versus temperature could then be plotted. Note that even during the quenching process, solidification of the previously formed solid could continue. The profile is thus considered as an overestimate of the solid fraction (underestimate of the remaining liquid fraction) prior to quenching. To estimate the liquidus temperature, differential thermal analysis (DTA) was used on heating rate 15°C/min for the steel S-1-DTA given in Table 1. The apparatus used is a SETARAM Thermobalance, with 10 mm height - 5 mm outer diameter alumina crucibles. The sample weight is around 500 mg. Note that other reactions, such as eutectic, were not detected with sufficient precision to be used.

2.2. EPMA Measurement on a Steel Alloy Sample

Electron Probe Micro-Analysis (EPMA) was carried out on a 3 cm × 5 cm × 1 cm sample extracted from the center of a 450 kg ingot casting (0.5 m width, 0.16 m thickness and 0.75 m height), in a region where no macrosegregation was observed. Its nominal composition, S-2, is given in Table 1. After polishing, EPMA was performed for manganese, phosphor and sulfur with a 5 μm diameter beam spot. The beam current was set to 0.5 A, the integration time was 0.5 s

and the measurement step was 50 μm. The analyzed area was 10 mm × 5 mm with a total number of probed points reaching 20 000. Sorting methods proposed in literature were used,[11] namely the Flemings-Gungor (FG) sort and the Weighted Interval Rank Sort (WIRS). FG is the simplest approach, in which all solutes are sorted independently as ascending order of the concentration. Only ascending order is employed since partition coefficients for manganese, phosphor and sulfur are less than unity. Each ordered data are assigned with a rank number from 1 to the total number of measurement points. Finally, the assigned rank is divided by the total number of points, providing with an estimation of the solid fraction. A chemical composition versus solid fraction curve could thus be drawn. WIRS takes into account the probed measurement data uncertainty in order to weight the compositions. The uncertainty is estimated by the difference between the average composition measured by EPMA and the nominal composition. The weighted compositional value is averaged at each probed position and the data are sorted according to the average weighted compositional values in ascending order. For a better analysis, the sorted data are finally averaged in each 0.01 solid fraction range.

3. Numerical Algorithm

Computations of advanced phase transformation paths are based on thermodynamic equilibrium calculations conducted with various conditions together with mass balances. The four basic approximations found in the literature[1–4] are reminded hereafter since they serve as the basis for the new combination derived in the present contribution.

3.1. Lever Rule (LR) Approximation

LR assumes complete mixing of all phases and thermodynamic equilibrium at interfaces, meaning that the chemical potential is equal in all phases for each chemical element. A close system is considered with constant mole, N_0, compositions, x_{i0}, and pressure P_0. It is defined by its n^p phases, including solid phases $s_1, s_2, \ldots$ plus a liquid phase l when present, *i.e.* p_j phases with $p_j = \{s_1, s_2, \ldots, l\}$ and $j = [1, n^p]$, as well as its total number of chemical elements, n^s, including both interstitial and substitutional elements. The system is at temperature $^{(k-1)}T$ with an initial phase fraction, $^{(k-1)}N^{p_j}$, at composition, $^{(k-1)}x_i^{p_j}$, with $p_j = \{s_1, s_2, \ldots, l\}$, $j = [1, n^p]$ and $i = [1, n^s]$. A small temperature decrease by ΔT is imposed to the system in order to compute its thermodynamic equilibrium at a lower temperature $^kT = {}^{(k-1)}T - \Delta T$. Mathematical formulation of LR first relies on equal chemical potential of each element respectively in all phases, $^k_{LR}\mu_i^{p_j}\left(^k_{LR}x_i^{p_j}\right)$. Considering mass conservation in the system, the set of equations are obtained as follows:

$$^k_{LR}\mu_i^{p_j}\left(^k_{LR}x_i^{p_j}\right) = {}_{LR}Cst_i$$

$$p_j = \{s_1, s_2, \ldots, l\}, j = [1, n^p], i = [1, n^s] \ldots (1)$$

$$\sum_{i=1}^{n^s} {}^k_{LR}x_i^{p_j} = 1 \qquad p_j = \{s_1, s_2, \ldots, l\}, j = [1, n^p], i = [1, n^s] \ldots (2)$$

Table 1. Nominal compositions (mass%) of steel alloys studied.

	Fe	C	Mn	S	Si	P	Al
S-1	Bal.	0.21	1.64	0.007	0.24	0.032	0.090
S-1-DTA	Bal.	0.20	1.50	0.007	0.22	0.020	0.024
S-2	Bal.	0.20	1.47	0.010	0.22	0.020	0.038

$$\sum_{j=1}^{n^p} {}_{LR}^{k} x_i^{p_j} \, {}_{LR}^{k} N^{p_j} = \sum_{j=1}^{n^p} {}^{(k-1)} x_i^{p_j} \, {}^{(k-1)} N^{p_j}$$

$$p_j = \{s_1, s_2, \ldots, 1\}, \; j = [1, n^p], \; i = [1, n^s] \; .. (3)$$

where ${}_{LR}^{k} N^{p_j}$ are phase fractions and ${}_{LR}^{k} x_i^{p_j}$ are compositions at equilibrium. The number of unknowns is $n^s(n^p + 1) + n^p$: $n^s n^p$ compositions, n^p phase fractions plus n^s constant ${}_{LR}Cst_i$. The number of equations is the same: $n^s n^p$ Eq. (1), n^p Eq. (2) plus n^s Eq. (3). In the flow chart given in **Fig. 1**, this corresponds to the dashed rectangle on the left-hand-side. It should be noticed that the temperature step ΔT is somewhat arbitrary and should be chosen small enough to ensure convergence of the entire transformation path. A single value equal to 0.05°C was used hereafter for all calculations.

3.2. Gulliver-Scheil (GS) Approximation

GS[1,2] assumes complete mixing of the liquid and thermodynamic equilibrium at the solid/liquid interface, with no diffusion of the chemical elements in the solid phases. The system is at temperature ${}^{(k-1)}T$ with an initial phase fraction, ${}^{(k-1)}N^{p_j}$, at average compositions, ${}^{(k-1)}\bar{x}_i^{p_j}$, with $p_j = \{s_1, s_2, \ldots, 1\}$, $j = [1, n^p]$ and $i = [1, n^s]$. A small temperature decrease by ΔT is imposed to a subsystem reduced to the above liquid, with initial phase fraction ${}^{(k-1)}N^1$ and compositions ${}^{(k-1)}x_i^1$, in order to compute a new thermodynamic equilibrium at a lower temperature, ${}^{k}T = {}^{(k-1)}T - \Delta T$, using Eqs. (1)–(3). In order to distinguish between LR (full equilibrium) and the present local equilibrium step for the remaining liquid, the output of the solution of Eqs. (1)–(3) are denoted with index EQ instead of LR: ${}_{EQ}^{k} N^{p_j}$ and ${}_{EQ}^{k} x_i^{p_j}$ with $p_j = \{s_1, s_2, \ldots, 1\}$, $j = [1, n^p]$ and $i = [1, n^s]$.
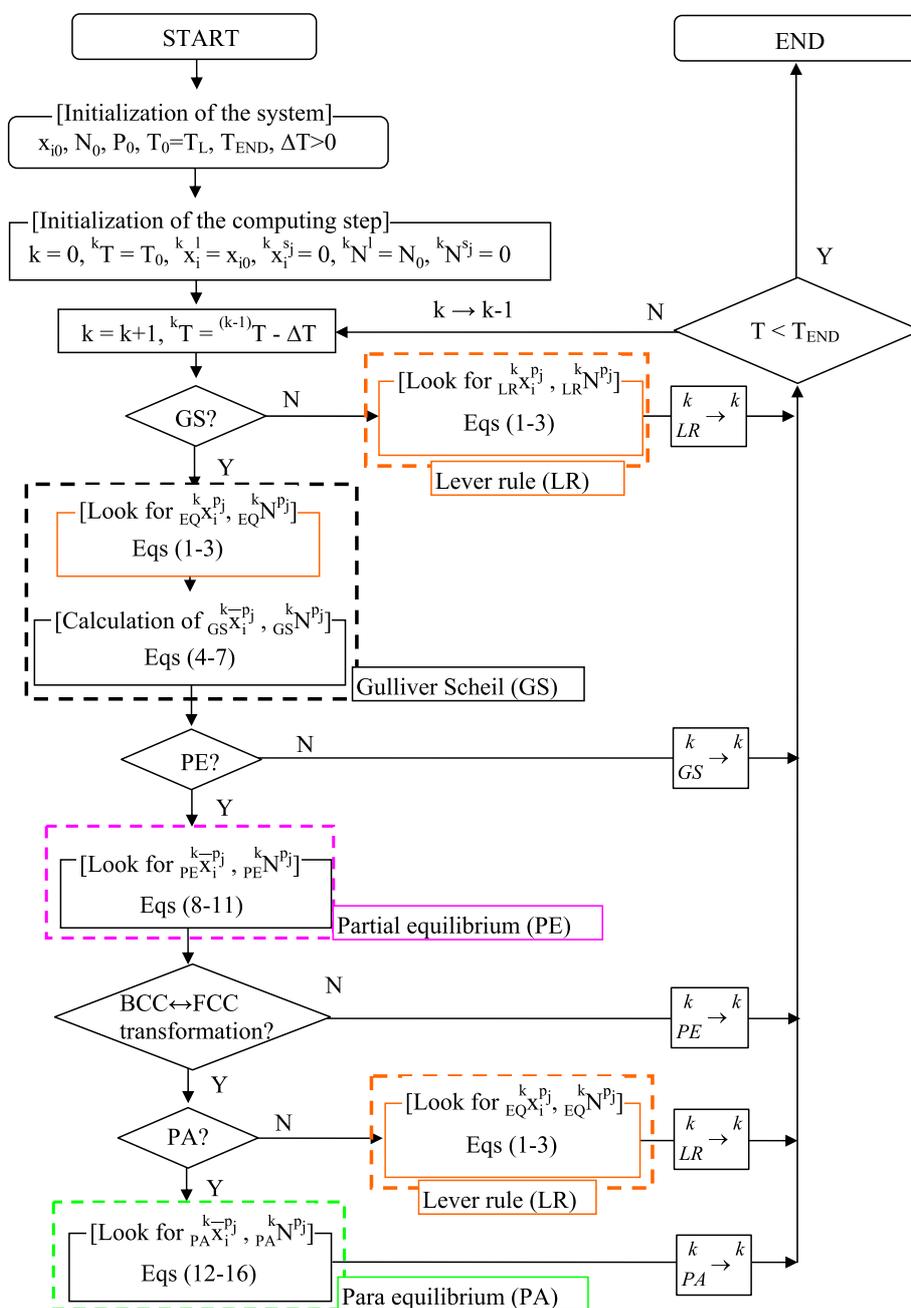

Fig. 1.   Schematic of the numerical schemes accounting for combinations of various thermodynamic approximations: lever rule (LR), Gulliver-Scheil (GS), partial-equilibrium (PE) and para-equilibrium (PA). (Online version in color.)

Because of the absence of diffusion in the solid phases under the GS approximation, the average solid composition of the entire system at temperature ^kT is directly computed by adding the fraction of solid formed during cooling of the subsystem to the already existing solid using:

$$_{GS}^k \overline{x}_i^{p_j \neq 1} = \left({}^{(k-1)}N^{p_j \neq 1}\, {}^{(k-1)}\overline{x}_i^{p_j \neq 1} + {}_{EQ}^kN^{p_j \neq 1}\, {}_{EQ}^kx_i^{p_j \neq 1} \right) /$$
$$\left({}^{(k-1)}N^{p_j \neq 1} + {}_{EQ}^kN^{p_j \neq 1} \right) \quad j = [1, n^p], i = [1, n^s] \ ... (4)$$

The new total fraction of the solid phases for the entire system is equal to:

$$_{GS}^k N^{p_j \neq 1} = {}^{(k-1)}N^{p_j \neq 1} + {}_{EQ}^kN^{p_j \neq 1} \quad j = [1, n^p], i = [1, n^s] \ ..... (5)$$

Liquid fraction and composition are simply given by the equilibrium solution:

$$_{GS}^k x_i^1 = {}_{EQ}^kx_i^1 \qquad\qquad i = [1, n^s] \ .... (6)$$

$$_{GS}^k N^1 = {}_{EQ}^kN^1 \qquad .... (7)$$

3.3. Partial-equilibrium (PE) Approximation

The PE approximation is intended to be used for systems with large differences in the diffusivity of chemical elements. This is typically the case in steels containing interstitial elements with high diffusivity and substitutional elements with low diffusivity. It is seen as an extension of the GS approximation and was initially developed for simulation of the solidification paths in steels[3,4] where carbon is interstitial and diffuses rapidly compared to $e.g.$, substitutional chromium. To simplify the problem, carbon is the only interstitial element considered in this study. Mathematical formulation of PE first relies on equal average chemical potential of carbon in all phases, $_{PE}^k\overline{\mu}_C^{p_j} \left(_{PE}^k\overline{x}_i^{p_j} \right)$. It also considers unchanged values for the average u-fractions of the substitutional elements defined by $_{PE}^k\overline{u}_{i\neq C}^{p_j} = {}_{PE}^k\overline{x}_{i\neq C}^{p_j} / \left(1 - {}_{PE}^k\overline{x}_C^{p_j}\right)$ with respect to the values provided by the last GS step at temperature ^kT for each phase participating to equilibrium, $_{GS}^k\overline{u}_{i\neq C}^{p_j} = {}_{GS}^k\overline{x}_{i\neq C}^{p_j} / \left(1 - {}_{GS}^k\overline{x}_C^{p_j}\right)$. These conditions are added the mass conservation of carbon and of all the substitutional elements over all participating phases considering the values provided by the last GS step at temperature ^kT. Thus, PE is initialized from a GS calculation as shown in Fig. 1. The above four considerations translate into:

$$_{PE}^k \overline{\mu}_C^{p_j} \left(_{PE}^k\overline{x}_i^{p_j} \right) = {}_{PE}Cst$$
$$p_j = \{s_1, s_2, ..., 1\}, j = [1, n^p], i = [1, n^s] .... (8)$$

$$_{PE}^k\overline{u}_{i\neq C}^{p_j} = {}_{GS}^k\overline{u}_{i\neq C}^{p_j} \quad p_j = \{s_1, s_2, ..., 1\}, j = [1, n^p], i = [1, n^s] ... (9)$$

$$\sum_{j=1}^{n^p} {}_{PE}^k\overline{x}_C^{p_j}\, {}_{PE}^kN^{p_j} = \sum_{j=1}^{n^p} {}_{GS}^k\overline{x}_C^{p_j}\, {}_{GS}^kN^{p_j}$$
$$p_j = \{s_1, s_2, ..., 1\}, j = [1, n^p] \ .... (10)$$

$$\sum_{i=1}^{n^s} {}_{PE}^k\overline{x}_{i\neq C}^{p_j}\, {}_{PE}^kN^{p_j} = \sum_{i=1}^{n^s} {}_{GS}^k\overline{x}_{i\neq C}^{p_j}\, {}_{GS}^kN^{p_j}$$
$$p_j = \{s_1, s_2, ..., 1\}, j = [1, n^p], i = [1, n^s] \ ..... (11)$$

The number of unknowns is $(n^s + 1)n^p + 1$: (n^sn^p) compositions, n^p phase fractions plus the constant $_{PE}Cst$. The number of equations is the same: n^p Eq. (8), $(n^s-1)n^p$ Eqs. (9), (10) plus n^p Eq. (11).

3.4. Para-equilibrium (PA) Approximation

On the basis of Hillert's idea,[8] the PA approximation was originally developed for a transformation taking place between solid phases with local equilibrium at the phase interface and frozen composition of substitutional elements. It permits to deal with solid phase transformation with the same u-fraction of substitutional elements and equality of chemical potential for instertitial elements. The condition on the interstitial element thus writes similarly as for the PE approximation with equal average chemical potentials among solid phases. This means that diffusion of interstitial elements is assumed very high, as for PE. For substitutional elements, condition is given on the summation of the product of the average chemical potential by the average u-fraction which is deduced from no driving force on the interface. A detailed derivation is given in Ref. 8). As stated before, it is chosen to consider a unique average u-fraction for each substitutional element in all the solid phases, $_{PE}^k\overline{u}_{i\neq C}^p$, $i = [1, n^s]$, its value being defined below. Finally, as for previous approximations, mass conservation of interstitial and substitutional elements over all solid phases must also be verified. Considering only carbon as the interstitial element, the following set of equations must thus be satisfied:

$$_{PA}^k\overline{\mu}_C^{p_j} \left(_{PA}^k\overline{x}_i^{p_j} \right) = {}_{PA}Cst1$$
$$p_j = \{s_1, s_2, ...\}, j = [1, n^p], i = [1, n^s] \ .... (12)$$

$$\sum_{j=1}^{n^p} {}_{PA}^k\overline{u}_{i\neq C}^{p_j}\, {}_{PA}^k\overline{\mu}_{i\neq C}^{p_j} \left(_{PA}^k\overline{x}_i^{p_j} \right) = {}_{PA}Cst2$$
$$p_j = \{s_1, s_2, ...\}, j = [1, n^p], i = [1, n^s] \ .... (13)$$

$$_{PA}^k\overline{u}_{i\neq C}^{p_j} = {}_{PE}^k\overline{u}_{i\neq C}^p \quad p_j = \{s_1, s_2, ...\}, j = [1, n^p], i = [1, n^s] \ ..... (14)$$

$$\sum_{j=1}^{n^p} {}_{PA}^k\overline{x}_C^{p_j}\, {}_{PA}^kN^{p_j} = \sum_{j=1}^{n^p} {}_{PE}^k\overline{x}_C^{p_j}\, {}_{PE}^kN^{p_j}$$
$$p_j = \{s_1, s_2, ...\}, j = [1, n^p] \ ...... (15)$$

$$\sum_{j=1}^{n^p} \sum_{i=1}^{n^s} {}_{PA}^k\overline{x}_{i\neq C}^{p_j}\, {}_{PA}^kN^{p_j} = \sum_{j=1}^{n^p} \sum_{i=1}^{n^s} {}_{PE}^k\overline{x}_{i\neq C}^{p_j}\, {}_{PE}^kN^{p_j}$$
$$p_j = \{s_1, s_2, ...\}, j = [1, n^p], i = [1, n^s] \ ..... (16)$$

The number of unknown compositions is $(n^s + 1)\, n^p + 2$: (n^sn^p) compositions, n^p phase fractions plus the constants $_{PA}Cst1$ and $_{PA}Cst2$. The number of equations is the same: n^p Eq. (12), n^p Eq. (13), $n^p(n^s-1)$ Eqs. (14), (15) plus Eq. (16). Comparing the set of equations for PA to PE approximations, the main difference appears through Eq. (13). In the literature, application of the PA approximation is usually limited to 2 solid phases. The above PA set of equations can be solved for a subsystem made of two solid phases $p_j = \{s_1, s_2\}$ undergoing a peritectic reaction, in which case this subsystem is extracted from a previous PE cal-

culation, thus explaining the index PE used in the above Eqs. (14)–(16). For the u-fraction, it is to be noticed that an average value is defined, ${}_{PE}^{k}\bar{u}_{i\neq C}^{p} = {}_{PE}^{k}\bar{x}_{i\neq C}^{p} / \left(1 - {}_{PE}^{k}\bar{x}_{C}^{p}\right)$ where

$${}_{PE}^{k}\bar{x}_{i\neq C}^{p} = \sum_{j=1}^{n^{p}} {}_{PE}^{k}\bar{x}_{i\neq C}^{p_{j}} {}_{PE}^{k}N^{p_{j}} / \sum_{j=1}^{n^{p}} {}_{PE}^{k}N^{p_{j}}.$$ It is thus computed for

the subsystem of the phases considered under PA. It is also worth noticing that when only solid phases coexist, a simple lever rule calculation can be used for initialisation.

Thus, PA provides with a local equilibrium condition at an interface that differs from LR or full equilibrium. PA and LR applied at a solid/solid interface can thus be combined with the PE approximation used to deal with a solid/liquid interface.

3.5. Numerical Scheme

The numerical scheme for a general cooling sequence during solidification is shown in Fig. 1. Several combinations of the above approximations are possible:

- LR (*i.e.*, not GS in Fig. 1). It obviously corresponds to full thermodynamic equilibrium transformation paths and is valid from a temperature higher than the liquidus temperature up to room temperature.
- GS (*i.e.*, not PE in Fig. 1). As explained above, it implies that all interstitial and substitutional elements in all solid phases are frozen, not permitting the peritectic reaction to take place. Because such approximation is difficult to maintain up to low temperature, a critical fraction of liquid (0.0001%) is chosen to stop the transformation, below which the average composition of all phases is kept constant: ${}_{GS}^{k}\bar{x}_{i}^{p_{j}\neq 1} = {}^{(k-1)}x_{i}^{p_{j}\neq 1}$ and ${}_{GS}^{k}N^{p_{j}\neq 1} = {}^{(k-1)}N^{p_{j}\neq 1}$.
- PE (*i.e.*, not BCC↔FCC in Fig. 1). Considered alone, it considers full equilibrium of interstitials while substitutional elements are frozen. This does change the solidification path compared to GS, yet still not permitting the peritectic reaction to occur.
- PE + LR (*i.e.*, not PA in Fig. 1). It keeps the PE approximation while handling the peritectic reaction by using a simple LR approximation among the δ-BCC and γ-FCC solid phases.[5] Note that the γ-FCC to α-BCC solid state transformation is considered in such situation.
- PE + PA (*i.e.*, PA in Fig. 1). This configuration provides with the most advanced configuration where the δ-BCC to γ-FCC peritectic transformation and the γ-FCC to α-BCC solid state transformation are both considered under PA conditions.

4. Application to Steel Alloys and Discussion

4.1. Solidification Path for S-1

The measured liquidus temperature by means of DTA and the calculated one are shown in **Table 2**. The calculated value based on thermodynamic equilibrium is slightly lower than measurement. It is yet within the uncertainty of the experimental method. During DTA, the temperature difference between the alloy sample and a reference sample is recorded during heating to reveal the latent heat required during melting. Such a phase transformation, however, needs a driving force leading to overheating of the sample

to transform the solid into liquid, and hence uncertainty in the determination of the liquidus temperature. The other possible reason is inherent to the precision of the thermocouples and the accuracy of the thermodynamic database. Overall, the comparison is thus considered as very good.

Figure 2(a) shows calculated solidification paths as a function of temperature for composition S-1. Figures 2(b) and 2(c) present the same results for smaller temperature intervals. Measurements data are added in Figs. 2(a) and 2(b). Differences clearly appear between computations using the various approximations. All simulations yet lie within the LR and GS curves. This was indeed expected since, in the absence of undercooling, LR and GS could be regarded as the two extreme thermodynamic limits with respect to solid state diffusion. Under LR, the total solid

Table 2. Liquidus temperature (°C) and onset temperature for the peritectic transformation (°C) deduced from DTA measurement and from the TCFE6 database[11] for alloy S-1 using various approximations.

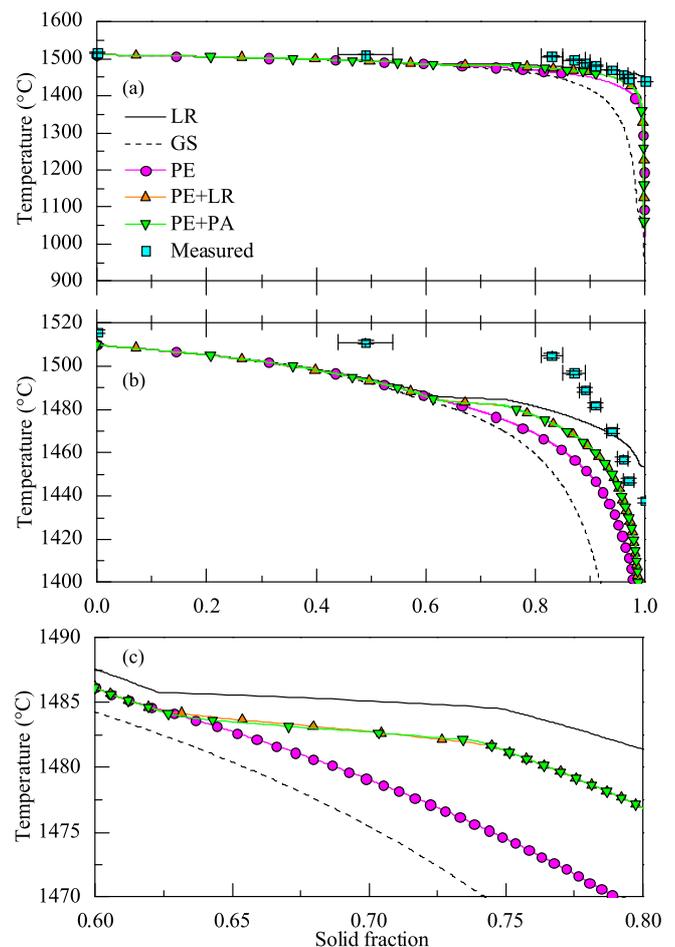| Liquidus	1 515 ± 5	1 511.45				
Peritectic transformation	1 490 ± 5	1 485.8	1 485.5	1 485.25	1484.6	1 484.25
	DTA	LR	GS	PE	PE + LR	PE + PA

Fig. 2. Solidification paths displayed for (a) the maximum solidification interval deduced from the predictions, (b) the experimental range, and (c) around the peritectic reaction. Measurement data are added for comparison. Steel S-1 (Table 1), 5 microsegregation models. (Online version in color.)

fraction increases within the smallest temperature range, *i.e.* [1 510°C, 1 453°C], while it is the largest for GS, *i.e.* [1 510°C, 958°C]. This is a common finding for alloy solidification. In the absence of diffusion in the solid phases and with segregation of elements in the liquid, solidification proceeds up to low temperature and can lead to the formation of additional intermetallic phases.

Figure 2(b) provides with a temperature range that permits a better comparison with experimental results. It is clear from this graph that even the most favorable simulation, *i.e.* LR, significantly underestimates the fraction of solid up to more than 90%, *i.e.* from the liquidus temperature up to 1 470°C. In the present situation, the procedures for collecting the experimental data can certainly be discussed. During solidification in the Bridgman furnace, thermosolutal convection could take place that would lead to a non-uniform alloy composition in the quenched sample, thus modifying the solidification path. This is a well-known phenomenon in upward Bridgman configuration, often reported in the literature for similar experimental set-up or even during in-situ observation.[12] Furthermore, as stated before, solidification of the solid phases can continue during quenching, thus overestimating the fraction of solid prior to quenching. Of course the approximations of the simulations are also of prime importance, among which the kinetics of the microstructures. As previously stated for fusion, solidification proceeds with diffusion limited kinetics. With undercooling, the microstructure forms with a sudden burst of the solid fraction just behind its growing interface, *i.e.* from its working temperature. Such sudden increase is reported by the observations, the fraction of solid increasing from 0 to more than 80% from the liquidus temperature, 1 515 ± 5°C, to 1 505 ± 5°C, *i.e.* within a 10°C interval.

Similar observation was reported in the literature. It was initially explained by considerations of the solute mass balance at the growth fronts[13] or more phenomenological analyses.[14] More sophisticated models were developed for this purpose, all taking into account growth undercooling of the microstructure due to limited diffusion in the liquid phase.[15] The analysis was made available in the presence of combined dendritic, peritectic and eutectic reactions.[16] However, it is still limited when considering multicomponent alloys.

A further magnification is provided in Fig. 2(c) around the peritectic reaction, *i.e.* the transformation of δ-BCC to γ-FCC. At around 1 485°C, all the curves present a slope change due to the formation of the peritectic γ-FCC phase. This is better seen in **Fig. 3** where the C and Mn composition of δ-BCC to γ-FCC are drawn for the same temperature interval as Fig. 2(c). Under LR, the δ-BCC to γ-FCC transformation starts at 1 485.5°C and end at 1 484.5°C. In the absence of diffusion in the solid phase (GS), the δ-BCC fraction is frozen at its composition up to room temperature. The set of conditions and equations for PE is shown to also freeze δ-BCC and its Mn composition while the C composition continues to evolve. However, it is not satisfying since peritectic reaction has to take place. For this reason, the PE + LR and PE + PA were computed. The difference between these two solidification paths can only be seen in Fig. 2(c). The present PE + PA transformation path differs very little from the original PE + LR treatment proposed by Chen *et al.*[5] One can yet mention the difference observed in Fig. 3. During the peritectic transformation under LR, PE + LR and PE + PA, the carbon composition decreases in both phases. In contrast, the manganese composition increases in both phases in case of LR and PE + PA, while it slightly decreases in case of PE + LR.
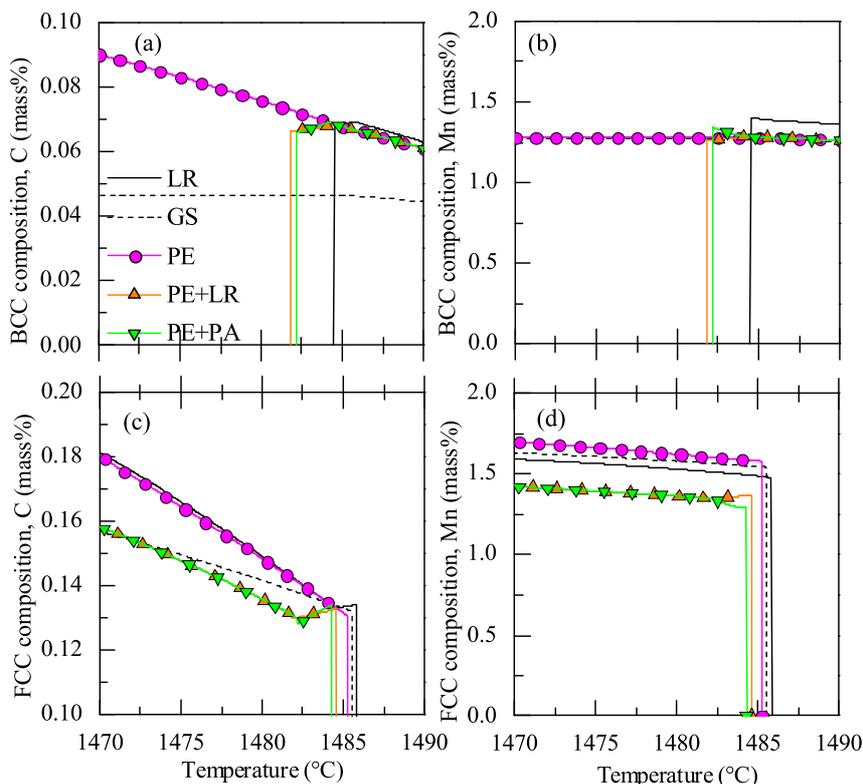

Fig. 3. Phase composition within the temperature range of the peritectic transformation for (left) carbon and (right) manganese in (top) BCC and (bottom) FCC phases. Steel S-1 (Table 1), 5 microsegregation models. (Online version in color.)

4.2. Transformation Path for S-2

In order to better analyze the PE + LR and PE + PA approximations, experimental and numerical studies were conducted on alloy composition S-2 given in Table 1. **Figure 4** shows the evolutions of BCC and FCC fractions when cooling the alloy from the liquid state up to room temperature. These evolutions are also given for intermetallics MnS, M$_3$P, and other phases in **Fig. 5**. Similar observations are found as for alloy S-1 upon primary δ-BCC solidification and the δ-BCC to γ-FCC peritectic transformation for the five approximations considered, *i.e.* δ-BCC is frozen below the peritectic temperature under GS and PE. Note in Figs. 5(a) and 5(b) the large differences found between the precipitation temperatures of the MnS and M$_3$P phases, respectively. The GS approximation predicts the lowest precipitation temperatures for these phases. It also reveals precipitation of Cementite and Graphite from the melt at around 950°C (Fig. 5(c)). Such large solidification interval is not likely to be achieved and this is clearly a limitation of the GS approximation. The PEs approximations also predict formation of the MnS and M$_3$P phases slightly above 1 000°C. At lower temperature, all phase fractions are locked under GS and PE. As stated before, this is coherent with solute mass balance analysis of frozen substitutional
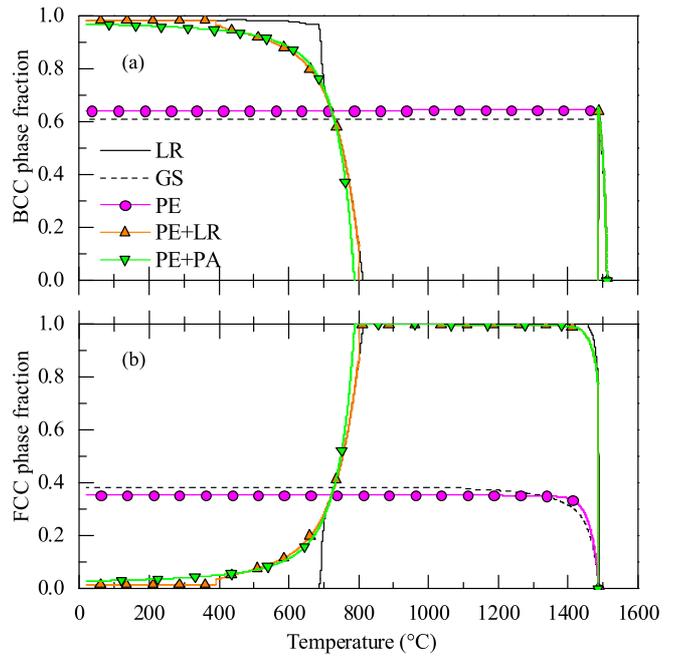

Fig. 4. Mass fraction of phases as a function of temperature for (top) δ-BCC and (bottom) γ-FCC. Steel S-2 (Table 1), 5 microsegregation models. (Online version in color.)
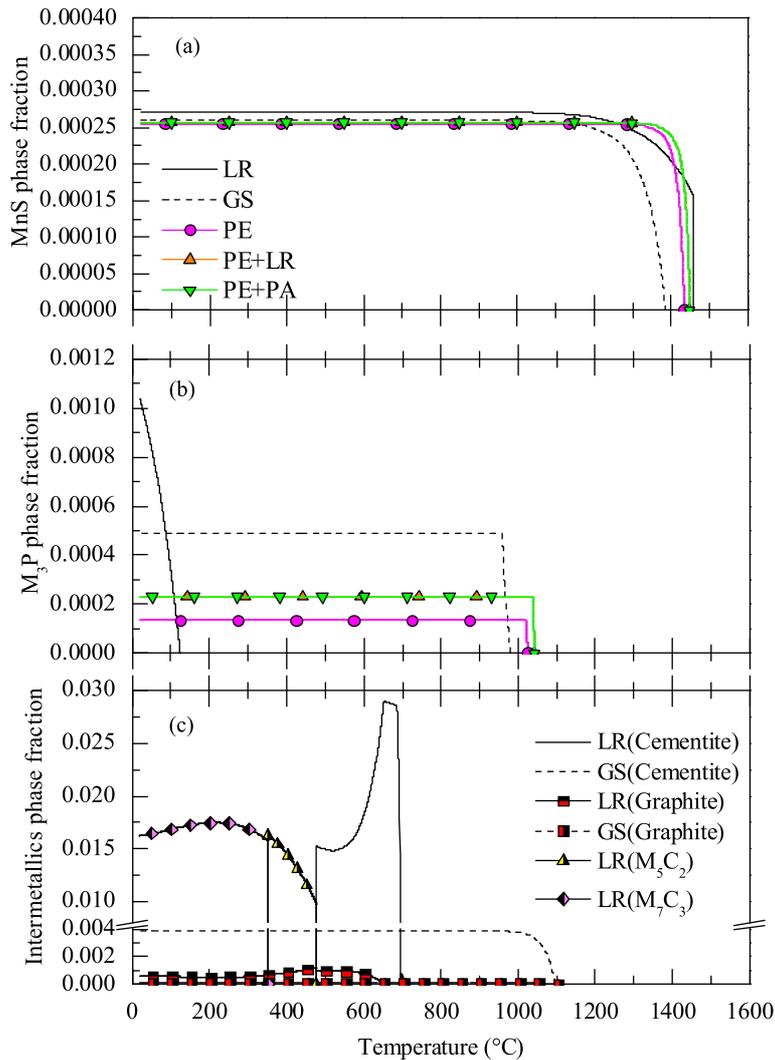

Fig. 5. Mass fraction of phases as a function of temperature for (top) MnS, (middle) M$_3$P and (bottom) other intermetallics. Steel S-2 (Table 1), 5 microsegregation models. (Online version in color.)

elements at phase interfaces.

When considering LR, PE + LR, and PE + PA, solid-solid interfaces are activated and phases can continue to evolve up to room temperature. These phase transformation paths are obviously more realistic since α-BCC (or α-ferrite) is classically found at room temperature. Figure 4 shows that the transformation starts below 800°C. Differences yet clearly appear on the curves, with LR prediction abruptly departing from the PE + LR and PE + PA curves at around 750°C with the transformation of γ-FCC into α-BCC. This behavior of the LR transformation path is only realistic if substitutional elements can rapidly equilibrate, leading to a full disappearance of γ-FCC. It also leads to the formation of Cementite, Graphite, M_5C_2 and M_7C_3 phases at lower temperatures as shown in Fig. 5(c). On the contrary, PE + LR and PE + PA show a continuous transformation of γ-FCC into α-BCC (Fig. 4) and no additional phases other

than MnS and M_3P. The latter paths are thus more realistic.

Figure 6 presents the BCC and FCC compositions in C and Mn predicted by the five approximations. Obviously, C is only frozen after solidification under GS while Mn is frozen for GS, PE and PE + PA. For LR and PE + LR, Mn composition continues to change after solidification. Consequently, Mn is fully transferred from δ-BCC to γ-FCC at room temperature, while austenite is not likely to be present anymore for this alloy. In case of PE + PA, the Mn content is maintained close to the nominal composition (1.47 mass%) in both FCC and BCC phases.

For a better assertion of the most meaningful combination of the thermodynamic approximations, EPMA measurements conducted on the S-2 composition is presented in **Fig. 7**. It presents the predicted average Mn composition at 20°C (left) and the interfacial Mn composition obtained during GS step denoted as $_{EQ}^k x_{Mn}^{p_j \neq 1}$ in Fig. 1 (right). One should
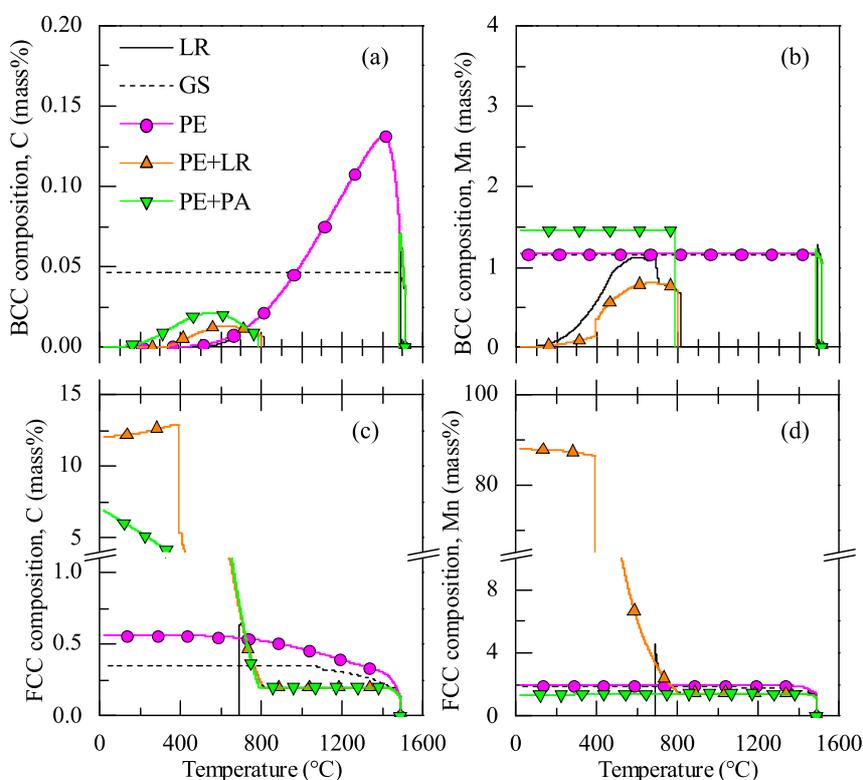

Fig. 6. Phase composition as a function of temperature for (left) carbon and (right) manganese in (top) BCC and (bottom) FCC phases. Steel S-2 (Table 1), 5 microsegregation models. (Online version in color.)
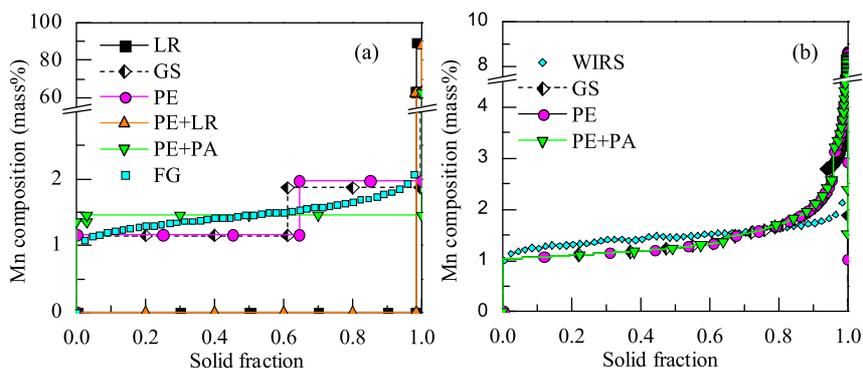

Fig. 7. Average Mn composition as a function of the mass fraction of solid with (left) FG and (right) WIRS sorting methods. Steel S-2 (Table 1), 5 microsegregation models. Parameters for the WIRS analysis are given in **Table 3**. (Online version in color.)

Table 3. Data for WIRS (mass%). σ is uncertainty, estimated as the difference between nominal composition and average composition of EPMA measurements.

	Mn	S	P
Min	0	0	0
σ	0.026	0.004	0.004

notice that the sample analyzed contains MnS, thus explaining the rapid increase of Mn content in the composition profiles for solid fraction above 0.95. The GS, PE and PE + PA approximations are found to provide better agreement with the measurements, using both the FG and WIRS sorting methods, *i.e.* when Mn diffusion is frozen. A clear change in the composition profile is yet predicted under GS, PE and PE + PA, when the solid fraction reaches around 0.65. It is due to the δ-BCC to γ-FCC transformation. According to previous considerations, the overall best agreement is thus found for the combination of PE + PA approximations.

5. Conclusion

(1) Combination of the partial- and para- equilibrium (PE + PA) thermodynamic approximations is proposed for the study of phase transformations in steels, from the liquid state to room temperature.

(2) Calculated solidification paths for multi-component alloys are discussed with respect to the peritectic transformation. It is found that, in case of PE + PA, the solidification path does not differ significantly from the lever rule (LR) and from the combination of the partial equilibrium plus lever rule (PE + LR) approximations.

(3) Differences with experimental results are discussed based on analyses of a sample processed by Bridgman solidification, showing the need for more accurate experimental results and removal of several modeling hypotheses (absence of microstructures kinetics and no treatment of limited diffusion in all phases).

(4) Regarding the solid state phase transformations, PE + PA is found to provide the most realistic composition profile of substitutional elements and evolution of the phase fractions. PE + PA is therefore recommended as the standard set of thermodynamic approximations to be used for the study of phase transformations in multicomponent steels.

REFERENCES

1) G. H. Gulliver: *J. Inst. Met.*, **9** (1913), 120.
2) E. Scheil: *Z. Metallkd.*, **34** (1942), 70.
3) Q. Chen and B. Sundman: *Mater. Trans.*, **43** (2002), 551.
4) H. Zhang, K. Nakajima, C. A. Gandin and J. He: *ISIJ Int.*, **53** (2013), 493.
5) Q. Chen, A. Engstrom, X.-G. Lu and B. Sundman: MCWASP-XI, ed. by Ch.-A. Gandin and M. Bellet, TMS, Warrendale, PA, (2006), 529.
6) Thermo-Calc TCCS Mnuals, Thermo-Calc Sftware AB, Stockholm, Sweden, (2013).
7) P. Shi: TCS steels/Fe-alloys Dtabase, V6.0, Thermo-Calc Software AB, Stockholm, Sweden, (2008).
8) M. Hillert: Phase Equilibria, Phase Diagrams and Phase Transformations, Cambridge University, UK, (1998), 358.
9) W. Kurz and D. J. Fisher: Fundamentals of Solidification, Trans Tech Publications Ltd, Switzerland, (1998), 7.
10) J. A. Dantzig and M. Rappaz: Solidification, EPFL Press, Lausanne, Switzerland, (2009), 17.
11) M. Ganesan and P. D. Lee: *Mater. Trans. A*, **36** (2005), 2191.
12) A. Bogno, H. Nguyen-Thi, G. Reinhart, B. Billia and J. Baruchel: *Acta Mater.*, **61** (2013), 1303.
13) J. A. Sarreal and G. J. Abbaschian: *Mater. Trans. A*, **17** (1986), 2063.
14) B. Giovanola and W. Kurz: *Mater. Trans. A*, **21** (1990), 260.
15) C. Y. Wang and C. Beckermann: *Mater. Sci. Eng. A*, **171** (1993), 199.
16) D. Tourret, Ch.-A. Gandin, T. Volkmann and D. M. Herlach: *Acta Mater.*, **59** (2011), 4665.